

MIT Open Access Articles

Exclusive production of $D[\textit{subscript s}] + D[\textit{subscript s}]^-$, $D[\textit{subscript s}]^ + D[\textit{subscript s}]^-$, and $D[\textit{subscript s}]^* + D[\textit{subscript s}]^{*-}$ via e^+e^- annihilation with initial-state radiation*

The MIT Faculty has made this article openly available. **Please share** how this access benefits you. Your story matters.

Citation: BABAR Collaboration et al. "Exclusive production of $D_{\textit{s}}^{+}D_{\textit{s}}^{-}$, $D_{\textit{s}}^{*+}D_{\textit{s}}^{-}$, and $D_{\textit{s}}^{*+}D_{\textit{s}}^{*-}$ via $e^{+}e^{-}$ annihilation with initial-state radiation." Physical Review D 82.5 (2010): 052004. © 2010 The American Physical Society.

As Published: <http://dx.doi.org/10.1103/PhysRevD.82.052004>

Publisher: American Physical Society

Persistent URL: <http://hdl.handle.net/1721.1/61327>

Version: Final published version: final published article, as it appeared in a journal, conference proceedings, or other formally published context

Terms of Use: Article is made available in accordance with the publisher's policy and may be subject to US copyright law. Please refer to the publisher's site for terms of use.



Exclusive production of $D_s^+ D_s^-$, $D_s^{*+} D_s^-$, and $D_s^{*+} D_s^{*-}$ via $e^+ e^-$ annihilation with initial-state radiation

P. del Amo Sanchez,¹ J. P. Lees,¹ V. Poireau,¹ E. Prencipe,¹ V. Tisserand,¹ J. Garra Tico,² E. Grauges,² M. Martinelli,^{3a,3b} A. Palano,^{3a,3b} M. Pappagallo,^{3a,3b} G. Eigen,⁴ B. Stugu,⁴ L. Sun,⁴ M. Battaglia,⁵ D. N. Brown,⁵ B. Hooberman,⁵ L. T. Kerth,⁵ Yu. G. Kolomensky,⁵ G. Lynch,⁵ I. L. Osipenko,⁵ T. Tanabe,⁵ C. M. Hawkes,⁶ A. T. Watson,⁶ H. Koch,⁷ T. Schroeder,⁷ D. J. Asgeirsson,⁸ C. Hearty,⁸ T. S. Mattison,⁸ J. A. McKenna,⁸ A. Khan,⁹ A. Randle-Conde,⁹ V. E. Blinov,¹⁰ A. R. Buzykaev,¹⁰ V. P. Druzhinin,¹⁰ V. B. Golubev,¹⁰ A. P. Onuchin,¹⁰ S. I. Serednyakov,¹⁰ Yu. I. Skovpen,¹⁰ E. P. Solodov,¹⁰ K. Yu. Todyshev,¹⁰ A. N. Yushkov,¹⁰ M. Bondioli,¹¹ S. Curry,¹¹ D. Kirkby,¹¹ A. J. Lankford,¹¹ M. Mandelkern,¹¹ E. C. Martin,¹¹ D. P. Stoker,¹¹ H. Atmacan,¹² J. W. Gary,¹² F. Liu,¹² O. Long,¹² G. M. Vitug,¹² C. Campagnari,¹³ T. M. Hong,¹³ D. Kovalskyi,¹³ J. D. Richman,¹³ A. M. Eisner,¹⁴ C. A. Heusch,¹⁴ J. Kroseberg,¹⁴ W. S. Lockman,¹⁴ A. J. Martinez,¹⁴ T. Schalk,¹⁴ B. A. Schumm,¹⁴ A. Seiden,¹⁴ L. O. Winstrom,¹⁴ C. H. Cheng,¹⁵ D. A. Doll,¹⁵ B. Echenard,¹⁵ D. G. Hitlin,¹⁵ P. Ongmongkolkul,¹⁵ F. C. Porter,¹⁵ A. Y. Rakitin,¹⁵ R. Andreassen,¹⁶ M. S. Dubrovin,¹⁶ G. Mancinelli,¹⁶ B. T. Meadows,¹⁶ M. D. Sokoloff,¹⁶ P. C. Bloom,¹⁷ W. T. Ford,¹⁷ A. Gaz,¹⁷ M. Nagel,¹⁷ U. Nauenberg,¹⁷ J. G. Smith,¹⁷ S. R. Wagner,¹⁷ R. Ayad,^{18,*} W. H. Toki,¹⁸ H. Jasper,¹⁹ T. M. Karbach,¹⁹ J. Merkel,¹⁹ A. Petzold,¹⁹ B. Spaan,¹⁹ K. Wacker,¹⁹ M. J. Kobel,²⁰ K. R. Schubert,²⁰ R. Schwierz,²⁰ D. Bernard,²¹ M. Verderi,²¹ P. J. Clark,²² S. Playfer,²² J. E. Watson,²² M. Andreotti,^{23a,23b} D. Bettoni,^{23a} C. Bozzi,^{23a} R. Calabrese,^{23a,23b} A. Cecchi,^{23a,23b} G. Cibinetto,^{23a,23b} E. Fioravanti,^{23a,23b} P. Franchini,^{23a,23b} E. Luppi,^{23a,23b} M. Munerato,^{23a,23b} M. Negrini,^{23a,23b} A. Petrella,^{23a,23b} L. Piemontese,^{23a} R. Baldini-Ferroli,²⁴ A. Calcaterra,²⁴ R. de Sangro,²⁴ G. Finocchiaro,²⁴ M. Nicolaci,²⁴ S. Pacetti,²⁴ P. Patteri,²⁴ I. M. Peruzzi,^{24,†} M. Piccolo,²⁴ M. Rama,²⁴ A. Zallo,²⁴ R. Contri,^{25a,25b} E. Guido,^{25a,25b} M. Lo Vetere,^{25a,25b} M. R. Monge,^{25a,25b} S. Passaggio,^{25a} C. Patrignani,^{25a,25b} E. Robutti,^{25a} S. Tosi,^{25a,25b} B. Bhuyan,²⁶ V. Prasad,²⁶ C. L. Lee,²⁷ M. Morii,²⁷ A. Adametz,²⁸ J. Marks,²⁸ U. Uwer,²⁸ F. U. Bernlochner,²⁹ M. Ebert,²⁹ H. M. Lacker,²⁹ T. Lueck,²⁹ A. Volk,²⁹ P. D. Dauncey,³⁰ M. Tibbetts,³⁰ P. K. Behera,³¹ U. Mallik,³¹ C. Chen,³² J. Cochran,³² H. B. Crawley,³² L. Dong,³² W. T. Meyer,³² S. Prell,³² E. I. Rosenberg,³² A. E. Rubin,³² A. V. Gritsan,³³ Z. J. Guo,³³ N. Arnaud,³⁴ M. Davier,³⁴ D. Derkach,³⁴ J. Firmino da Costa,³⁴ G. Grosdidier,³⁴ F. Le Diberder,³⁴ A. M. Lutz,³⁴ B. Malaescu,³⁴ A. Perez,³⁴ P. Roudeau,³⁴ M. H. Schune,³⁴ J. Serrano,³⁴ V. Sordini,^{34,‡} A. Stocchi,³⁴ L. Wang,³⁴ G. Wormser,³⁴ D. J. Lange,³⁵ D. M. Wright,³⁵ I. Bingham,³⁶ C. A. Chavez,³⁶ J. P. Coleman,³⁶ J. R. Fry,³⁶ E. Gabathuler,³⁶ R. Gamet,³⁶ D. E. Hutchcroft,³⁶ D. J. Payne,³⁶ C. Touramanis,³⁶ A. J. Bevan,³⁷ F. Di Lodovico,³⁷ R. Sacco,³⁷ M. Sigamani,³⁷ G. Cowan,³⁸ S. Paramesvaran,³⁸ A. C. Wren,³⁸ D. N. Brown,³⁹ C. L. Davis,³⁹ A. G. Denig,⁴⁰ M. Fritsch,⁴⁰ W. Gradl,⁴⁰ A. Hafner,⁴⁰ K. E. Alwyn,⁴¹ D. Bailey,⁴¹ R. J. Barlow,⁴¹ G. Jackson,⁴¹ G. D. Lafferty,⁴¹ T. J. West,⁴¹ J. Anderson,⁴² R. Cenci,⁴² A. Jawahery,⁴² D. A. Roberts,⁴² G. Simi,⁴² J. M. Tuggle,⁴² C. Dallapiccola,⁴³ E. Salvati,⁴³ R. Cowan,⁴⁴ D. Dujmic,⁴⁴ G. Sciolla,⁴⁴ M. Zhao,⁴⁴ D. Lindemann,⁴⁵ P. M. Patel,⁴⁵ S. H. Robertson,⁴⁵ M. Schram,⁴⁵ P. Biassoni,^{46a,46b} A. Lazzaro,^{46a,46b} V. Lombardo,^{46a} F. Palombo,^{46a,46b} S. Stracka,^{46a,46b} L. Cremaldi,⁴⁷ R. Godang,^{47,§} R. Kroeger,⁴⁷ P. Sonnek,⁴⁷ D. J. Summers,⁴⁷ X. Nguyen,⁴⁸ M. Simard,⁴⁸ P. Taras,⁴⁸ G. De Nardo,^{49a,49b} D. Monorchio,^{49a,49b} G. Onorato,^{49a,49b} C. Sciacca,^{49a,49b} G. Raven,⁵⁰ H. L. Snoek,⁵⁰ C. P. Jessop,⁵¹ K. J. Knoepfel,⁵¹ J. M. LoSecco,⁵¹ W. F. Wang,⁵¹ L. A. Corwin,⁵² K. Honscheid,⁵² R. Kass,⁵² J. P. Morris,⁵² N. L. Blount,⁵³ J. Brau,⁵³ R. Frey,⁵³ O. Igonkina,⁵³ J. A. Kolb,⁵³ R. Rahmat,⁵³ N. B. Siney,⁵³ D. Strom,⁵³ J. Strube,⁵³ E. Torrence,⁵³ G. Castelli,^{54a,54b} E. Feltresi,^{54a,54b} N. Gagliardi,^{54a,54b} M. Margoni,^{54a,54b} M. Morandin,^{54a} M. Posocco,^{54a} M. Rotondo,^{54a} F. Simonetto,^{54a,54b} R. Stroili,^{54a,54b} E. Ben-Haim,⁵⁵ G. R. Bonneaud,⁵⁵ H. Briand,⁵⁵ G. Calderini,⁵⁵ J. Chauveau,⁵⁵ O. Hamon,⁵⁵ Ph. Leruste,⁵⁵ G. Marchiori,⁵⁵ J. Ocariz,⁵⁵ J. Prendki,⁵⁵ S. Sitt,⁵⁵ M. Biasini,^{56a,56b} E. Manoni,^{56a,56b} A. Rossi,^{56a,56b} C. Angelini,^{57a,57b} G. Batignani,^{57a,57b} S. Bettarini,^{57a,57b} M. Carpinelli,^{57a,57b,||} G. Casarosa,^{57a,57b} A. Cervelli,^{57a,57b} F. Forti,^{57a,57b} M. A. Giorgi,^{57a,57b} A. Lusiani,^{57a,57c} N. Neri,^{57a,57b} E. Paoloni,^{57a,57b} G. Rizzo,^{57a,57b} J. J. Walsh,^{57a} D. Lopes Pegna,⁵⁸ C. Lu,⁵⁸ J. Olsen,⁵⁸ A. J. S. Smith,⁵⁸ A. V. Telnov,⁵⁸ F. Anulli,^{59a} E. Baracchini,^{59a,59b} G. Cavoto,^{59a} R. Faccini,^{59a,59b} F. Ferrarotto,^{59a} F. Ferroni,^{59a,59b} M. Gaspero,^{59a,59b} L. Li Gioi,^{59a} M. A. Mazzoni,^{59a} G. Piredda,^{59a} F. Renga,^{59a,59b} T. Hartmann,⁶⁰ T. Leddig,⁶⁰ H. Schröder,⁶⁰ R. Waldi,⁶⁰ T. Adye,⁶¹ B. Franek,⁶¹ E. O. Olaiya,⁶¹ F. F. Wilson,⁶¹ S. Emery,⁶² G. Hamel de Monchenault,⁶² G. Vasseur,⁶² Ch. Yèche,⁶² M. Zito,⁶² M. T. Allen,⁶³ D. Aston,⁶³ D. J. Bard,⁶³ R. Bartoldus,⁶³ J. F. Benitez,⁶³ C. Cartaro,⁶³ M. R. Convery,⁶³ J. Dorfan,⁶³ G. P. Dubois-Felsmann,⁶³ W. Dunwoodie,⁶³ R. C. Field,⁶³ M. Franco Sevilla,⁶³ B. G. Fulsom,⁶³ A. M. Gabareen,⁶³ M. T. Graham,⁶³ P. Grenier,⁶³ C. Hast,⁶³ W. R. Innes,⁶³ M. H. Kelsey,⁶³ H. Kim,⁶³ P. Kim,⁶³ M. L. Kocian,⁶³ D. W. G. S. Leith,⁶³ S. Li,⁶³ B. Lindquist,⁶³ S. Luitz,⁶³ V. Luth,⁶³ H. L. Lynch,⁶³ D. B. MacFarlane,⁶³ H. Marsiske,⁶³ D. R. Muller,⁶³ H. Neal,⁶³ S. Nelson,⁶³ C. P. O'Grady,⁶³ I. Ofte,⁶³ M. Perl,⁶³ T. Pulliam,⁶³ B. N. Ratcliff,⁶³ A. Roodman,⁶³

A. A. Salnikov,⁶³ V. Santoro,⁶³ R. H. Schindler,⁶³ J. Schwiening,⁶³ A. Snyder,⁶³ D. Su,⁶³ M. K. Sullivan,⁶³ S. Sun,⁶³ K. Suzuki,⁶³ J. M. Thompson,⁶³ J. Va'vra,⁶³ A. P. Wagner,⁶³ M. Weaver,⁶³ C. A. West,⁶³ W. J. Wisniewski,⁶³ M. Wittgen,⁶³ D. H. Wright,⁶³ H. W. Wulsin,⁶³ A. K. Yarritu,⁶³ C. C. Young,⁶³ V. Ziegler,⁶³ X. R. Chen,⁶⁴ W. Park,⁶⁴ M. V. Purohit,⁶⁴ R. M. White,⁶⁴ J. R. Wilson,⁶⁴ S. J. Sekula,⁶⁵ M. Bellis,⁶⁶ P. R. Burchat,⁶⁶ A. J. Edwards,⁶⁶ T. S. Miyashita,⁶⁶ S. Ahmed,⁶⁷ M. S. Alam,⁶⁷ J. A. Ernst,⁶⁷ B. Pan,⁶⁷ M. A. Saeed,⁶⁷ S. B. Zain,⁶⁷ N. Guttman,⁶⁸ A. Soffer,⁶⁸ P. Lund,⁶⁹ S. M. Spanier,⁶⁹ R. Eckmann,⁷⁰ J. L. Ritchie,⁷⁰ A. M. Ruland,⁷⁰ C. J. Schilling,⁷⁰ R. F. Schwitters,⁷⁰ B. C. Wray,⁷⁰ J. M. Izen,⁷¹ X. C. Lou,⁷¹ F. Bianchi,^{72a,72b} D. Gamba,^{72a,72b} M. Pelliccioni,^{72a,72b} M. Bomben,^{73a,73b} L. Lanceri,^{73a,73b} L. Vitale,^{73a,73b} N. Lopez-March,⁷⁴ F. Martinez-Vidal,⁷⁴ D. A. Milanes,⁷⁴ A. Oyanguren,⁷⁴ J. Albert,⁷⁵ Sw. Banerjee,⁷⁵ H. H. F. Choi,⁷⁵ K. Hamano,⁷⁵ G. J. King,⁷⁵ R. Kowalewski,⁷⁵ M. J. Lewczuk,⁷⁵ I. M. Nugent,⁷⁵ J. M. Roney,⁷⁵ R. J. Sobie,⁷⁵ T. J. Gershon,⁷⁶ P. F. Harrison,⁷⁶ T. E. Latham,⁷⁶ E. M. T. Puccio,⁷⁶ H. R. Band,⁷⁷ S. Dasu,⁷⁷ K. T. Flood,⁷⁷ Y. Pan,⁷⁷ R. Prepost,⁷⁷ C. O. Vuosalo,⁷⁷ and S. L. Wu⁷⁷

(BABAR Collaboration)

¹Laboratoire d'Annecy-le-Vieux de Physique des Particules (LAPP), Université de Savoie, CNRS/IN2P3, F-74941 Annecy-Le-Vieux, France

²Universitat de Barcelona, Facultat de Física, Departament ECM, E-08028 Barcelona, Spain

^{3a}INFN Sezione di Bari, I-70126 Bari, Italy

^{3b}Dipartimento di Fisica, Università di Bari, I-70126 Bari, Italy

⁴University of Bergen, Institute of Physics, N-5007 Bergen, Norway

⁵Lawrence Berkeley National Laboratory and University of California, Berkeley, California 94720, USA

⁶University of Birmingham, Birmingham, B15 2TT, United Kingdom

⁷Ruhr Universität Bochum, Institut für Experimentalphysik 1, D-44780 Bochum, Germany

⁸University of British Columbia, Vancouver, British Columbia, Canada V6T 1Z1

⁹Brunel University, Uxbridge, Middlesex UB8 3PH, United Kingdom

¹⁰Budker Institute of Nuclear Physics, Novosibirsk 630090, Russia

¹¹University of California at Irvine, Irvine, California 92697, USA

¹²University of California at Riverside, Riverside, California 92521, USA

¹³University of California at Santa Barbara, Santa Barbara, California 93106, USA

¹⁴University of California at Santa Cruz, Institute for Particle Physics, Santa Cruz, California 95064, USA

¹⁵California Institute of Technology, Pasadena, California 91125, USA

¹⁶University of Cincinnati, Cincinnati, Ohio 45221, USA

¹⁷University of Colorado, Boulder, Colorado 80309, USA

¹⁸Colorado State University, Fort Collins, Colorado 80523, USA

¹⁹Technische Universität Dortmund, Fakultät Physik, D-44221 Dortmund, Germany

²⁰Technische Universität Dresden, Institut für Kern- und Teilchenphysik, D-01062 Dresden, Germany

²¹Laboratoire Leprince-Ringuet, CNRS/IN2P3, Ecole Polytechnique, F-91128 Palaiseau, France

²²University of Edinburgh, Edinburgh EH9 3JZ, United Kingdom

^{23a}INFN Sezione di Ferrara, I-44100 Ferrara, Italy

^{23b}Dipartimento di Fisica, Università di Ferrara, I-44100 Ferrara, Italy

²⁴INFN Laboratori Nazionali di Frascati, I-00044 Frascati, Italy

^{25a}INFN Sezione di Genova, I-16146 Genova, Italy

^{25b}Dipartimento di Fisica, Università di Genova, I-16146 Genova, Italy

²⁶Indian Institute of Technology Guwahati, Guwahati, Assam, 781 039, India

²⁷Harvard University, Cambridge, Massachusetts 02138, USA

²⁸Universität Heidelberg, Physikalisches Institut, Philosophenweg 12, D-69120 Heidelberg, Germany

²⁹Humboldt-Universität zu Berlin, Institut für Physik, Newtonstrasse 15, D-12489 Berlin, Germany

³⁰Imperial College London, London, SW7 2AZ, United Kingdom

³¹University of Iowa, Iowa City, Iowa 52242, USA

³²Iowa State University, Ames, Iowa 50011-3160, USA

³³Johns Hopkins University, Baltimore, Maryland 21218, USA

³⁴Laboratoire de l'Accélérateur Linéaire, IN2P3/CNRS et Université Paris-Sud 11,

Centre Scientifique d'Orsay, B. P. 34, F-91898 Orsay Cedex, France

³⁵Lawrence Livermore National Laboratory, Livermore, California 94550, USA

³⁶University of Liverpool, Liverpool L69 7ZE, United Kingdom

³⁷Queen Mary, University of London, London, E1 4NS, United Kingdom

³⁸University of London, Royal Holloway and Bedford New College, Egham, Surrey TW20 0EX, United Kingdom

³⁹University of Louisville, Louisville, Kentucky 40292, USA

- ⁴⁰*Johannes Gutenberg-Universität Mainz, Institut für Kernphysik, D-55099 Mainz, Germany*
⁴¹*University of Manchester, Manchester M13 9PL, United Kingdom*
⁴²*University of Maryland, College Park, Maryland 20742, USA*
⁴³*University of Massachusetts, Amherst, Massachusetts 01003, USA*
⁴⁴*Massachusetts Institute of Technology, Laboratory for Nuclear Science, Cambridge, Massachusetts 02139, USA*
⁴⁵*McGill University, Montréal, Québec, Canada H3A 2T8*
^{46a}*INFN Sezione di Milano, I-20133 Milano, Italy*
^{46b}*Dipartimento di Fisica, Università di Milano, I-20133 Milano, Italy*
⁴⁷*University of Mississippi, University, Mississippi 38677, USA*
⁴⁸*Université de Montréal, Physique des Particules, Montréal, Québec, Canada H3C 3J7*
^{49a}*INFN Sezione di Napoli, I-80126 Napoli, Italy*
^{49b}*Dipartimento di Scienze Fisiche, Università di Napoli Federico II, I-80126 Napoli, Italy*
⁵⁰*NIKHEF, National Institute for Nuclear Physics and High Energy Physics, NL-1009 DB Amsterdam, The Netherlands*
⁵¹*University of Notre Dame, Notre Dame, Indiana 46556, USA*
⁵²*The Ohio State University, Columbus, Ohio 43210, USA*
⁵³*University of Oregon, Eugene, Oregon 97403, USA*
^{54a}*INFN Sezione di Padova, I-35131 Padova, Italy*
^{54b}*Dipartimento di Fisica, Università di Padova, I-35131 Padova, Italy*
⁵⁵*Laboratoire de Physique Nucléaire et de Hautes Energies, IN2P3/CNRS, Université Pierre et Marie Curie-Paris6, Université Denis Diderot-Paris7, F-75252 Paris, France*
^{56a}*INFN Sezione di Perugia, I-06100 Perugia, Italy*
^{56b}*Dipartimento di Fisica, Università di Perugia, I-06100 Perugia, Italy*
^{57a}*INFN Sezione di Pisa, I-56127 Pisa, Italy*
^{57b}*Dipartimento di Fisica, Università di Pisa, I-56127 Pisa, Italy*
^{57c}*Scuola Normale Superiore di Pisa, I-56127 Pisa, Italy*
⁵⁸*Princeton University, Princeton, New Jersey 08544, USA*
^{59a}*INFN Sezione di Roma, I-00185 Roma, Italy*
^{59b}*Dipartimento di Fisica, Università di Roma La Sapienza, I-00185 Roma, Italy*
⁶⁰*Universität Rostock, D-18051 Rostock, Germany*
⁶¹*Rutherford Appleton Laboratory, Chilton, Didcot, Oxon, OX11 0QX, United Kingdom*
⁶²*CEA, Irfu, SPP, Centre de Saclay, F-91191 Gif-sur-Yvette, France*
⁶³*SLAC National Accelerator Laboratory, Stanford, California 94309 USA*
⁶⁴*University of South Carolina, Columbia, South Carolina 29208, USA*
⁶⁵*Southern Methodist University, Dallas, Texas 75275, USA*
⁶⁶*Stanford University, Stanford, California 94305-4060, USA*
⁶⁷*State University of New York, Albany, New York 12222, USA*
⁶⁸*Tel Aviv University, School of Physics and Astronomy, Tel Aviv, 69978, Israel*
⁶⁹*University of Tennessee, Knoxville, Tennessee 37996, USA*
⁷⁰*University of Texas at Austin, Austin, Texas 78712, USA*
⁷¹*University of Texas at Dallas, Richardson, Texas 75083, USA*
^{72a}*INFN Sezione di Torino, I-10125 Torino, Italy*
^{72b}*Dipartimento di Fisica Sperimentale, Università di Torino, I-10125 Torino, Italy*
^{73a}*INFN Sezione di Trieste, I-34127 Trieste, Italy*
^{73b}*Dipartimento di Fisica, Università di Trieste, I-34127 Trieste, Italy*
⁷⁴*IFIC, Universitat de Valencia-CSIC, E-46071 Valencia, Spain*
⁷⁵*University of Victoria, Victoria, British Columbia, Canada V8W 3P6*
⁷⁶*Department of Physics, University of Warwick, Coventry CV4 7AL, United Kingdom*
⁷⁷*University of Wisconsin, Madison, Wisconsin 53706, USA*
(Received 2 August 2010; published 29 September 2010)

We perform a study of exclusive production of $D_s^+ D_s^-$, $D_s^{*+} D_s^-$, and $D_s^{*+} D_s^{*-}$ final states in initial-state-radiation events from $e^+ e^-$ annihilations at a center-of-mass energy near 10.58 GeV, to search for charmonium 1^{--} states. The data sample corresponds to an integrated luminosity of 525 fb⁻¹ and was recorded by the BABAR experiment at the PEP-II storage ring. The $D_s^+ D_s^-$, $D_s^{*+} D_s^-$, and $D_s^{*+} D_s^{*-}$ mass

*Present address: Temple University, Philadelphia, PA 19122, USA.

†Also with Università di Perugia, Dipartimento di Fisica, Perugia, Italy.

‡Also with Università di Roma La Sapienza, I-00185 Roma, Italy.

§Present address: University of South Alabama, Mobile, AL 36688, USA.

||Also with Università di Sassari, Sassari, Italy.

spectra show evidence of the known ψ resonances. Limits are extracted for the branching ratios of the decays $X(4260) \rightarrow D_s^{(*)+} D_s^{(*)-}$.

DOI: 10.1103/PhysRevD.82.052004

PACS numbers: 14.40.Pq, 13.25.Gv, 13.66.Bc

I. INTRODUCTION

The surprising discovery of new states decaying to $J/\psi \pi^+ \pi^-$ [1,2] has renewed interest in the field of charmonium spectroscopy, since not all the new resonances are easy to accommodate in the quark model. Specifically, the *BABAR* experiment discovered a broad state, $X(4260)$, decaying to $J/\psi \pi^+ \pi^-$, in the initial-state-radiation (ISR) reaction $e^+ e^- \rightarrow \gamma_{\text{ISR}} X(4260)$. Its quantum numbers $J^{PC} = 1^{--}$ are inferred from the single virtual-photon production. Enhancements in the $\psi(2S) \pi^+ \pi^-$ mass distribution at 4.36 GeV/ c^2 [3,4] and 4.66 GeV/ c^2 [4] have been observed for the reaction $e^+ e^- \rightarrow \gamma_{\text{ISR}} \psi(2S) \pi^+ \pi^-$. Charmonium states at these masses would be expected [5,6] to decay predominantly to $D\bar{D}$, $D^* \bar{D}$, or $D^* \bar{D}^*$. It is peculiar that the decay rate to the hidden charm final state $J/\psi \pi^+ \pi^-$ is much larger for the $X(4260)$ than for the higher-mass charmonium states (radial excitations) [7]. Many theoretical interpretations for the $X(4260)$ have been proposed, including unconventional scenarios: quark-antiquark gluon hybrids [8], baryonium [9], tetraquarks [10], and hadronic molecules [11]. If the $X(4260)$ were a diquark-antidiquark state $[cs][\bar{c}\bar{s}]$, as proposed by Maiani *et al.* [10], this state would predominantly decay to $D_s^+ D_s^-$. For a discussion and a list of references see, for example, Ref. [12].

In this paper, we present a study of the ISR production of $D_s^+ D_s^-$, $D_s^{*+} D_s^-$, and $D_s^{*+} D_s^{*-}$ [13] final states, and search for evidence of charmonium states and resonant structures. This follows earlier *BABAR* measurements of the cross section of $D\bar{D}$ [14] and of $D^* \bar{D}$ and $D^* \bar{D}^*$ production [15] and studies of these final states [16,17] by the Belle Collaboration. Recently the CLEO Collaboration [18] studied $e^+ e^-$ annihilation to $D_s^+ D_s^-$, $D_s^{*+} D_s^-$, and $D_s^{*+} D_s^{*-}$ final states at center-of-mass energies from threshold up to 4.3 GeV GeV/ c^2 . In the present analysis we extend these measurements up to 6.2 GeV/ c^2 .

This paper is organized as follows. A short description of the *BABAR* experiment is given in Sec. II, and data selection is described in Sec. III. In Secs. IV, V, and VI we present studies of the $D_s^+ D_s^-$, $D_s^{*+} D_s^-$, and $D_s^{*+} D_s^{*-}$ final states, respectively. Fits to the three final states are described in Sec. VII, and in Sec. VIII we present limits on the decay of the $X(4260)$ to $D_s^{(*)+} D_s^{(*)-}$. A summary and conclusions are found in Sec. IX.

II. THE BABAR EXPERIMENT

This analysis is based on a data sample of 525 fb $^{-1}$ recorded mostly at the $Y(4S)$ resonance and 40 MeV below the resonance by the *BABAR* detector at the PEP-II

asymmetric-energy $e^+ e^-$ storage rings. The sample includes also 15.9 fb $^{-1}$ and 31.2 fb $^{-1}$ collected at the $Y(2S)$ and $Y(3S)$ respectively, and 4.4 fb $^{-1}$ above the $Y(4S)$ resonances. The *BABAR* detector is described in detail elsewhere [19]. We mention here only the components of the detector that are used in the present analysis. Charged particles are detected and their momenta measured with a combination of a cylindrical drift chamber (DCH) and a silicon vertex tracker (SVT), both operating within a 1.5 T magnetic field of a superconducting solenoid. Information from a ring-imaging Cherenkov detector is combined with specific ionization measurements from the SVT and DCH to identify charged kaon and pion candidates. The efficiency for kaon identification is 90% while the rate for a kaon being misidentified as a pion is 2%. Photon energies are measured with a CsI(Tl) electromagnetic calorimeter (EMC).

III. DATA SELECTION

For each candidate event, we first reconstruct a $D_s^+ D_s^-$ pair. While one of the D_s^+ is required to decay to $K^+ K^- \pi^+$, we include three different decay channels for the second D_s^- (see Table I). D_s^{*+} decays are reconstructed via their decay $D_s^{*+} \rightarrow D_s^+ \gamma$.

For all final states, events are retained if the number of well-measured charged tracks having a transverse momentum greater than 0.1 GeV/ c is exactly equal to the total number of charged daughter particles. EMC clusters with a minimum energy of 30 MeV that are not associated with a charged track are identified as photons. Candidates for the decay $\pi^0 \rightarrow \gamma\gamma$ are kinematically constrained to the π^0 mass. For $K_S^0 \rightarrow \pi^+ \pi^-$ candidates we apply vertex and mass constraints. The tracks corresponding to the charged daughters of each D_s^+ candidate are constrained to come from a common vertex. Reconstructed D_s^+ candidates with a fit probability greater than 0.1% are retained. Each $D_s^+ D_s^-$ pair is refit to a common vertex with the constraint that the pair originates from the $e^+ e^-$ interaction region. Only candidates with a χ^2 fit probability greater than 0.1% are retained. For each event we consider all combinations.

TABLE I. Reconstructed decay channels for the two D_s^\pm mesons in each event.

Channel	First D_s decay	Second D_s decay
(1)	$K^+ K^- \pi^+$	$K^+ K^- \pi^-$
(2)	$K^+ K^- \pi^+$	$K^+ K^- \pi^- \pi^0$
(3)	$K^+ K^- \pi^+$	$K_S^0 K^-$

ISR Monte Carlo (MC) [20] events for each final state are fully simulated using the GEANT4 detector simulation package [21], and they are processed through the same reconstruction and analysis chain as the data.

We select D_s^+ and D_s^{*+} candidates using the reconstructed D_s^+ mass and the mass difference, which for $D_s^+ \rightarrow K^+ K^- \pi^+$ is defined as $\Delta m(D_s^+ \gamma) \equiv m(K^+ K^- \pi^+ \gamma) - m(K^+ K^- \pi^+)$. The D_s^+ parameters are obtained by fitting the relevant mass spectra using a polynomial for the background and a single Gaussian for the signal. For D_s^{*+} , we use the PDG [22] mass and a Gaussian width $\sigma = 6 \text{ MeV}/c^2$ obtained by MC simulations. Events are selected within $\pm 2.0\sigma$ from the fitted central values. The $D_s^{(*)+}$ candidate three-momentum is determined from the summed three-momenta of its decay particles. The nominal $D_s^{(*)+}$ mass [22] is used to compute the energy component of its four-momentum.

The ISR photon is preferentially emitted at small angles with respect to the beam axis, and it escapes detection in the majority of ISR events ($\approx 87\%$). Consequently, the ISR photon is treated as a missing particle. We define the squared mass M_{rec}^2 recoiling against the $D_s^+ D_s^-$, $D_s^{*+} D_s^-$, and $D_s^{*+} D_s^{*-}$ systems using the four-momenta of the beam particles p_{e^\pm} and of the reconstructed $D_s^{(*)\pm}$ $p_{D_s^{(*)\pm}}$:

$$M_{\text{rec}}^2 \equiv (p_{e^-} + p_{e^+} - p_{D_s^{(*)+}} - p_{D_s^{(*)-}})^2. \quad (1)$$

This quantity should peak near zero for both ISR events and for exclusive production of $e^+ e^- \rightarrow D_s^{(*)+} D_s^{(*)-}$. For exclusive production, the $D_s^{(*)+} D_s^{(*)-}$ mass distribution peaks at the kinematic limit. We reject exclusive events by requiring the $D_s^{(*)+} D_s^{(*)-}$ mass to be below $6.2 \text{ GeV}/c^2$ and select ISR candidates by requiring $|M_{\text{rec}}^2| < 0.8 \text{ GeV}^2/c^4$.

We allow additional π^0 and photon candidates due to radiative or background photons. This introduces multiple candidates in the reconstruction of the different channels. For channel (1)–(2) ambiguities, each $[K^+ K^- \pi^+ (\pi^0)]$ combination is considered as a candidate for both channels. For all channels, each $[D_s^+, D_s^-, (\gamma), (\gamma)]$ combination is considered as a candidate for $D_s^+ D_s^-$, $D_s^{*+} D_s^-$, and $D_s^{*+} D_s^{*-}$.

To discriminate among the different D_s^+ channels and $D_s^{(*)+} D_s^{(*)-}$ final states, and to separate signal from background, we make use of a likelihood ratio test:

$$L = \sum_{i=1}^N \log(PDF_i^S) - \sum_{i=1}^N \log(PDF_i^B), \quad (2)$$

where N is the number of discriminating variables, while PDF_i^S and PDF_i^B are normalized distributions describing signal and background, respectively. Signal PDF_i^S are obtained from MC simulations. Background PDF_i^B are obtained from the data. Since the ISR signal is very small compared to the entire data set of candidates ($< 0.1\%$),

we use the data as the background model by relaxing all the selection criteria, except $m(D_s^{(*)+} D_s^{(*)-}) < 6.2 \text{ GeV}/c^2$.

The discriminating variables used in the likelihood ratio are the following:

- (i) The number of additional π^0 candidates in the event. For decay channel (2) this number is computed after removing the π^0 from D_s^+ decay. This distribution is expected to peak at zero for signal events.
- (ii) The residual energy in the calorimeter, which is computed after removing any ISR photon candidate, identified by a center-of-mass energy greater than $2.0 \text{ GeV}/c^2$. For $D_s^{*+} D_s^-$ and $D_s^{*+} D_s^{*-}$ final states, the γ from D_s^{*+} decays is excluded from the residual energy calculation. This distribution is expected to peak at zero for signal events.
- (iii) The distribution of $\cos\theta^*$, where θ^* is the polar angle of the $D_s^{(*)+} D_s^{(*)-}$ system in the center-of-mass frame which peaks at ± 1 for ISR events.
- (iv) The momentum distribution of the π^0 from the D_s^+ for decay channel (2).
- (v) The γ energy distribution from D_s^{*+} for $D_s^{*+} D_s^-$ and $D_s^{*+} D_s^{*-}$ final states.

For each D_s^+ decay channel (1)–(3) and for each $D_s^+ D_s^-$, $D_s^{*+} D_s^-$, and $D_s^{*+} D_s^{*-}$ final state, we produce a likelihood ratio test according to Eq. (2) and apply empirically determined cuts on L in order to reduce the background and minimize the signal loss.

IV. STUDY OF THE $D_s^+ D_s^-$ FINAL STATE

MC studies demonstrate that the main background to the $D_s^+ D_s^-$ final state is from $D_s^{*+} D_s^-$ events, which have a larger cross section. Therefore, we eliminate $D_s^{*+} D_s^-$ candidates if they are also identified as $D_s^{*+} D_s^-$ candidates. MC simulations show that this veto rejects about 14% of the true $D_s^+ D_s^-$ final states and that the residual background is consistent with $D_s^{*+} D_s^-$ feedthrough.

Figure 1(a) shows the M_{rec}^2 distribution for the selected $D_s^+ D_s^-$ candidates, summed over the D_s^+ decay channels (1)–(3). The peak centered at zero is evidence for the ISR process. To determine the number of signal and

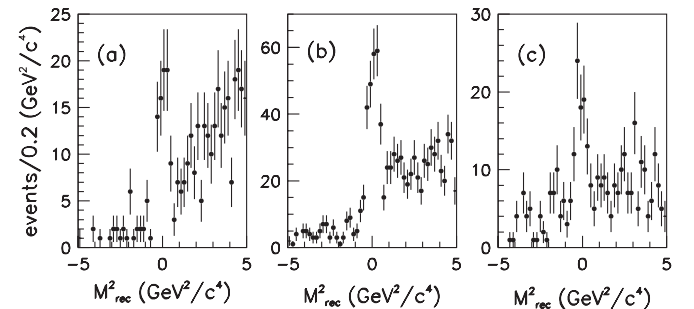


FIG. 1. Distributions of M_{rec}^2 for the (a) $D_s^+ D_s^-$, (b) $D_s^{*+} D_s^-$, and (c) $D_s^{*+} D_s^{*-}$ final states.

background events, we perform a χ^2 fit to the M_{rec}^2 distribution. The background is approximated by a 2nd order polynomial. The signal line shape is taken from $D_s^+ D_s^-$ MC simulations. The resulting yield and the fitted purity P , defined as $P = N_{\text{signal}}/(N_{\text{signal}} + N_{\text{background}})$ are summarized in Table II.

The $D_s^+ D_s^-$ mass spectrum, presented in Fig. 2(a), shows a threshold enhancement at the position of the $\psi(4040)$ and a small enhancement around 4.26 GeV/c².

We make use of the Gaussian functions to describe the presence of the peaking backgrounds. The $D_s^+ D_s^-$ background, taken from M_{rec}^2 sideband events ($1.5 < |M_{\text{rec}}^2| < 3.5$ GeV²/c⁴), is fitted to a sum of a Gaussian function and a 3rd order polynomial. The fitted $D_s^+ D_s^-$ mass spectrum for these events, normalized to the background estimated from the fit to the M_{rec}^2 distribution, is presented as the shaded distribution in Fig. 2(a).

The $D_s^+ D_s^-$ reconstruction efficiency and the mass resolution for each channel have been studied in the mass region between 4.25 and 6.25 GeV/c². The $D_s^+ D_s^-$ mass resolution is similar for decay channels (1) and (3) and slightly worse for decay channel (2) (by ≈ 1 MeV/c²). It increases with $D_s^+ D_s^-$ mass from 3.5 to 5.5 MeV/c² in the mass region of the ψ resonances (< 5 GeV/c²). The mass-dependent reconstruction efficiency for the $D_s^+ D_s^-$ decay channel i ($i = 1, 3$), $\epsilon_i(m_{D_s^+ D_s^-})$, evaluated at five different mass values, is parametrized in terms of a 2nd order polynomial, and scaled to account for the product branching fractions for each channel, \mathcal{B}_i [22], given in Table I,

$$\epsilon_i^{\mathcal{B}}(m_{D_s^+ D_s^-}) = \epsilon_i(m_{D_s^+ D_s^-}) \times \mathcal{B}_i. \quad (3)$$

These values are weighted by $N_i(m_{D_s^+ D_s^-})$, the number of $D_s^+ D_s^-$ candidates in decay channel i , to compute the average efficiency as a function of $m_{D_s^+ D_s^-}$,

$$\epsilon^{\mathcal{B}}(m_{D_s^+ D_s^-}) = \frac{\sum_{i=1}^3 N_i(m_{D_s^+ D_s^-})}{\sum_{i=1}^3 \frac{N_i(m_{D_s^+ D_s^-})}{\epsilon_i^{\mathcal{B}}(m_{D_s^+ D_s^-})}}. \quad (4)$$

The $\epsilon^{\mathcal{B}}$ function for $D_s^+ D_s^-$ is shown in Fig. 3(a). The three $D_s^+ D_s^-$ decay channels, after correcting for efficiency and branching fractions, have yields that are consistent within statistical errors.

TABLE II. Number of signal ISR candidates and purities for the different final states calculated in the range $|M_{\text{rec}}^2| < 0.8$ GeV²/c⁴.

Final state	Signal + background	Purity (%)
$D_s^+ D_s^-$	81	65.4 ± 5.3
$D_s^{*+} D_s^-$	286	67.1 ± 2.8
$D_s^{*+} D_s^{*-}$	105	54.3 ± 4.9

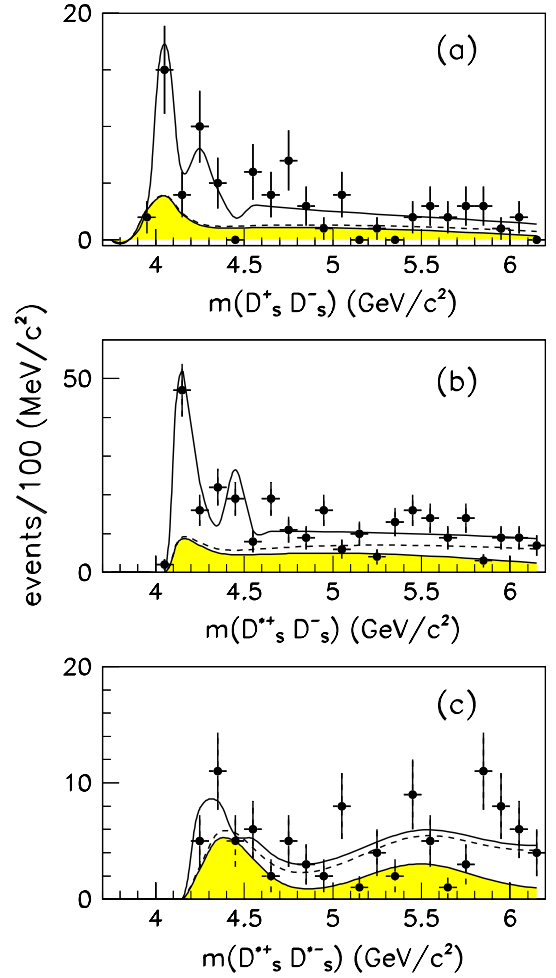


FIG. 2 (color online). The observed (a) $D_s^+ D_s^-$, (b) $D_s^{*+} D_s^-$, and (c) $D_s^{*+} D_s^{*-}$ mass spectra. The shaded areas show the background derived from fits to the M_{rec}^2 sidebands. The dashed lines indicate the sum of this background and the coherent background. The solid lines are the results from the fit described in Sec. VII.

The $D_s^+ D_s^-$ cross section is computed using

$$\sigma_{e^+ e^- \rightarrow D_s^+ D_s^-}(m_{D_s^+ D_s^-}) = \frac{dN/dm_{D_s^+ D_s^-}}{\epsilon^{\mathcal{B}}(m_{D_s^+ D_s^-}) d\mathcal{L}/dm_{D_s^+ D_s^-}}, \quad (5)$$

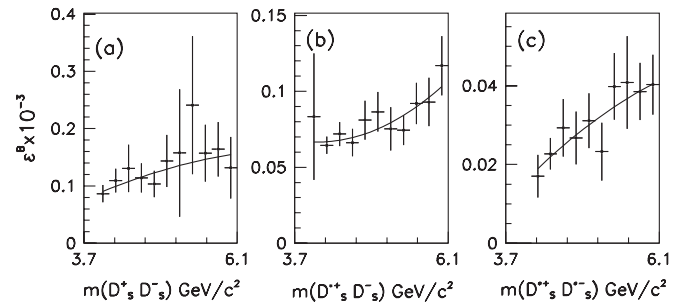


FIG. 3. Weighted efficiencies $\epsilon^{\mathcal{B}}$ for (a) $D_s^+ D_s^-$, (b) $D_s^{*+} D_s^-$, and (c) $D_s^{*+} D_s^{*-}$.

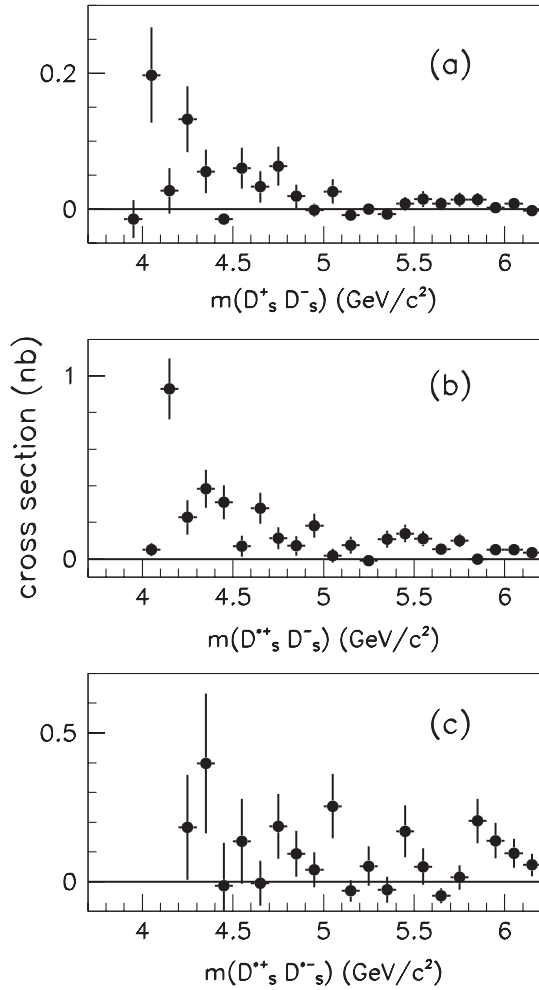


FIG. 4. Cross section for $e^+e^- \rightarrow$ (a) $D_s^+ D_s^-$, (b) $D_s^{*+} D_s^-$, and (c) $D_s^{*+} D_s^{*-}$. The error bars correspond to statistical errors only.

where $dN/dm_{D_s^+ D_s^-}$ is the background-subtracted yield. The differential luminosity is computed as [23]

$$\frac{d\mathcal{L}}{dm_{D_s^+ D_s^-}} = \mathcal{L} \frac{2m_{D_s^+ D_s^-}}{s} \frac{\alpha}{\pi x} (\ln(s/m_e^2) - 1)(2 - 2x + x^2), \quad (6)$$

where s is the square of the e^+e^- center-of-mass energy, α is the fine-structure constant, $x = 1 - m_{D_s^+ D_s^-}^2/s$, m_e is the

TABLE III. Systematic uncertainties (in %) for the evaluation of the $D_s^+ D_s^-$, $D_s^{*+} D_s^-$, and $D_s^{*+} D_s^{*-}$ cross sections.

Source	$D_s^+ D_s^-$	$D_s^{*+} D_s^-$	$D_s^{*+} D_s^{*-}$
Background subtraction	18.0	4.2	4.9
Branching fractions	10.0	10.0	10.0
Particle identification	5.0	5.0	5.0
Tracking efficiency	1.4	1.4	1.4
π^0 's and γ	1.1	2.9	4.7
Likelihood selection	8.7	4.0	
Total	23	13	13

electron mass, and \mathcal{L} is the integrated luminosity of 525 fb^{-1} . The cross section for $D_s^+ D_s^-$ is shown in Fig. 4(a). This result can be compared with QCD calculations in Ref. [24], which predict a vanishing cross section near $5 \text{ GeV}/c^2$.

The list of systematic uncertainties for the $D_s^+ D_s^-$ cross section is summarized in Table III and it is evaluated to be 23%. It includes contributions from particle identification, tracking, photon and π^0 reconstruction efficiencies, background estimates, branching fractions, and the criteria to select the final state. All contributions are added in quadrature. The $D_s^+ D_s^-$ systematic error is dominated by the uncertainty in the veto of the $D_s^{*+} D_s^-$ events.

V. STUDY OF THE $D_s^{*+} D_s^-$ FINAL STATE

A similar analysis is carried out for the $D_s^{*+} D_s^-$. Figure 5(a) shows the $\Delta m(D_s^+ \gamma)$ distributions for $D_s^{*+} D_s^-$ candidates passing the ISR requirements described in Sec. III. We also require the presence of a reconstructed D_s^- .

The M_{rec}^2 distribution for $D_s^{*+} D_s^-$ candidates is shown in Fig. 1(b) where a clear signal of ISR production is observed. The number of ISR candidates and sample purity are summarized in Table II.

The $D_s^{*+} D_s^-$ mass spectrum and background are shown in Fig. 2(b) and is dominated by the $\psi(4160)$ resonance. The $D_s^{*+} D_s^-$ mass resolution is similar for the three decay channels and increases with $D_s^{*+} D_s^-$ mass from 7 to 8 MeV/c^2 in the mass region of the ψ resonances. The weighted efficiency ϵ^B is shown in Fig. 3(b). The $D_s^{*+} D_s^-$ cross section is calculated using the method described in Sec. IV for $D_s^+ D_s^-$. The result is shown in Fig. 4(b). The overall systematic error for the cross section is 13% and is dominated by the uncertainties in the branching fractions [22] (see Table III).

VI. STUDY OF THE $D_s^{*+} D_s^{*-}$ FINAL STATE

For the selection of $D_s^{*+} D_s^{*-}$ candidates, we do not make use of the likelihood test described in the previous sections

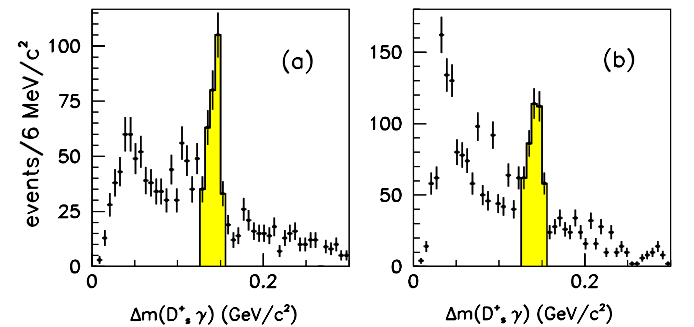


FIG. 5 (color online). Δm distributions for D_s^{*+} candidates after applying the $|M_{\text{rec}}^2| < 0.8 \text{ GeV}^2/c^4$ and $m(D_s^{(*)+} D_s^{(*)-}) < 6.2 \text{ GeV}/c^2$ selections, for the (a) $D_s^{*+} D_s^-$, and (b) $D_s^{*+} D_s^{*-}$ samples. The shaded regions indicate the ranges used to select the D_s^+ candidates.

because no improvement for the signal to background ratio is obtained. Instead, we require the two photon invariant mass $m(\gamma\gamma)$ to lie outside the π^0 window.

The ambiguity in the γ 's assignment to D_s^{*+} or D_s^{*-} is resolved by choosing the $D_s^+ \gamma D_s^- \gamma$ combinations with both $D_s^{(*)\pm}$ masses closest to the expected value. Figure 1(c) shows the resulting M_{rec}^2 distribution which shows clear evidence for the signal final state produced in interactions with ISR. For the selected the ISR signal candidates, we show the $\Delta m(D_s^+ \gamma)$ distribution (two combinations per event) in Fig. 5(b). The resulting event yield and purity are summarized in Table II.

The $D_s^{*+} D_s^{*-}$ mass spectrum and background are shown in Fig. 2(c). Because of the presence of structures, the background in this case is fitted using a 3rd order polynomial and two Gaussians. Monte Carlo studies indicate that an important part of this background is due to the $D_s^{*+} D_s^-$ final state plus a random background γ . The $D_s^{*+} D_s^{*-}$ mass resolution is similar for the three decay channels. It increases with $D_s^{*+} D_s^{*-}$ mass from 9 to 11 MeV/ c^2 in the mass region of the ψ resonances. The weighted efficiency ϵ^B is shown in Fig. 3(c). The $D_s^{*+} D_s^{*-}$ cross section shown in Fig. 4(c) is calculated using the same method used to compute the $D_s^+ D_s^-$ cross section. The overall uncertainty for the cross section is 13% and is dominated by the uncertainties on the $D_s^{(*)\pm}$ branching fractions (see Table III).

The $D_s^+ D_s^-$, $D_s^{*+} D_s^-$, and $D_s^{*+} D_s^{*-}$ cross sections, where they overlap, are in good agreement with CLEO [18] measurements.

VII. FIT TO THE MASS SPECTRA

Unbinned maximum likelihood fits are performed separately to the $D_s^+ D_s^-$, $D_s^{*+} D_s^-$, and $D_s^{*+} D_s^{*-}$ mass spectra. The likelihood function used is

$$L = f \epsilon^B(m) |P(m) + c_1 W_1(m) e^{i\phi_1} + \dots + c_n W_n(m) e^{i\phi_n}|^2 + B(m)(1 - f), \quad (7)$$

where m is the $D_s^{(*)+} D_s^{(*)-}$ mass, c_i and ϕ_i are free parameters, $W_i(m)$ are P -wave relativistic Breit-Wigner distributions [22], $P(m)$ represents the nonresonant

TABLE IV. $D_s^+ D_s^-$, $D_s^{*+} D_s^-$, and $D_s^{*+} D_s^{*-}$ fit fractions (in %). Errors are statistical only.

Resonance	$D_s^+ D_s^-$	Fraction $D_s^{*+} D_s^-$	$D_s^{*+} D_s^{*-}$
$P(m)$	11 ± 5	27 ± 5	71 ± 20
$\psi(4040)$	62 ± 21		
$\psi(4160)$	23 ± 26	53 ± 8	
$\psi(4415)$	6 ± 11	4 ± 2	5 ± 12
$X(4260)$	0.5 ± 3.0	18 ± 24	11 ± 16
Sum	103 ± 36	102 ± 26	87 ± 28

contribution, $B(m)$ is the background described in Sec. IV, $\epsilon^B(m)$ is the weighted efficiency, and f is the signal fraction fixed to the values obtained fitting the M_{rec}^2 distributions. In this way we allow interference between the resonances and the nonresonant contribution $P(m)$. The shape of the nonresonant contribution $P(m)$ is unknown; we therefore parametrize it in a simple way as

$$P(m) = C(m)(a + bm), \quad (8)$$

where $C(m)$ is the phase space function for $D_s^{(*)+} D_s^{(*)-}$, and a and b are free parameters. The size of the nonresonant production is determined by the fit.

The mass and width of the $\psi(4040)$, $\psi(4160)$, $\psi(4415)$ and $X(4260)$ are fixed to the values reported in [22]. Resolution effects can be ignored since the widths of the resonances are much larger than the experimental resolution.

The three $D_s^+ D_s^-$, $D_s^{*+} D_s^-$, and $D_s^{*+} D_s^{*-}$ likelihood functions are computed with different thresholds, efficiencies, purities, backgrounds, and numbers of contributing resonances appropriate for each final state. The results of this fits are compared to the data in Fig. 2, both the total fitted yield as well as the coherent nonresonant contribution, $|P(m)|^2$, ignoring any interference effects.

The fraction for each resonant contribution i is defined by the following expression:

$$f_i = \frac{|c_i|^2 \int |W_i(m)|^2 dm}{\sum_{j,k} c_j c_k^* \int W_j(m) W_k^*(m) dm}. \quad (9)$$

The fractions f_i do not necessarily add up to 1 because of interference between amplitudes. The error for each fraction has been evaluated by propagating the full covariance matrix obtained by the fit. The resulting fit fractions are given in Table IV. The $D_s^+ D_s^-$ cross section is dominated by the $\psi(4040)$ resonance, and the $D_s^{*+} D_s^-$ cross section by the $\psi(4160)$ resonance. The $D_s^{*+} D_s^{*-}$ cross section shows little resonance production. The fits to the $D_s^+ D_s^-$, $D_s^{*+} D_s^-$, and $D_s^{*+} D_s^{*-}$ mass spectra include the $X(4260)$ resonance, which is allowed to interfere with all the other terms. In all cases, the $X(4260)$ fraction is consistent with zero. We note that the weak enhancement around 4.26 GeV/ c^2 in the $D_s^+ D_s^-$ mass spectrum is described by the fit in terms of interference between the $\psi(4040)$ and $\psi(4160)$ resonances.

VIII. LIMITS ON $X(4260)$

The $X(4260)$ yields are used to compute the cross section times branching fraction, to be compared with a BABAR measurement of the $J/\psi \pi^+ \pi^-$ final state [2]. The fractions from the fits reported in Table IV are converted to yields which are divided by the mass-dependent ϵ^B efficiency and the integrated luminosity. Systematic errors due to the mass and the width of the $\psi(4040)$, $\psi(4160)$, $\psi(4415)$, and $X(4260)$ resonances are evaluated

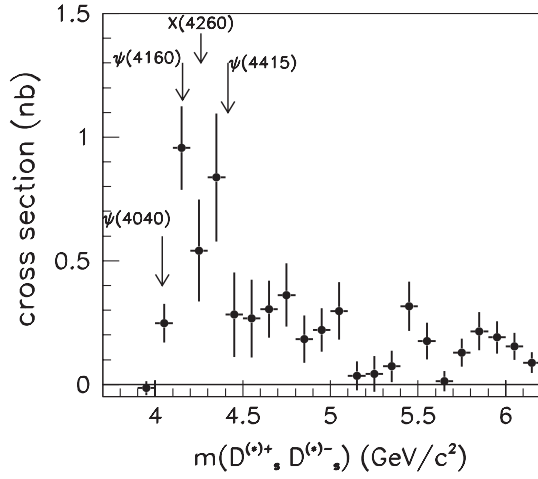


FIG. 6. Sum of $e^+e^- \rightarrow D_s^+ D_s^-$, $e^+e^- \rightarrow D_s^{*+} D_s^-$, and $e^+e^- \rightarrow D_s^{*+} D_s^{*-}$ cross sections. Errors are statistical only. The arrows indicate the positions of the different ψ resonances and the $X(4260)$.

by varying the masses and widths by their uncertainty in the fit. The size of the background contributions is varied within the statistical error, and the meson radii in the Breit-Wigner terms [25] are varied between 0 and 2.5 GeV^{-1} . Statistical and systematic errors are added in quadrature. We obtain

$$\frac{\mathcal{B}(X(4260) \rightarrow D_s^+ D_s^-)}{\mathcal{B}(X(4260) \rightarrow J/\psi \pi^+ \pi^-)} < 0.7, \quad (10)$$

$$\frac{\mathcal{B}(X(4260) \rightarrow D_s^{*+} D_s^-)}{\mathcal{B}(X(4260) \rightarrow J/\psi \pi^+ \pi^-)} < 44, \quad (11)$$

and

$$\frac{\mathcal{B}(X(4260) \rightarrow D_s^{*+} D_s^{*-})}{\mathcal{B}(X(4260) \rightarrow J/\psi \pi^+ \pi^-)} < 30, \quad (12)$$

at the 95% confidence level.

IX. TOTAL CROSS SECTION AND CONCLUSION

The sum of the $e^+e^- \rightarrow D_s^+ D_s^-$, $e^+e^- \rightarrow D_s^{*+} D_s^-$, and $e^+e^- \rightarrow D_s^{*+} D_s^{*-}$ cross sections is shown in Fig. 6; the arrows indicate the position of the different ψ resonances

and the $X(4260)$. At the $X(4260)$ mass, there is a local minimum, similar to the measured cross section for hadron production in e^+e^- annihilation [22].

In conclusion, we have studied the exclusive ISR production of the $D_s^+ D_s^-$, $D_s^{*+} D_s^-$, and $D_s^{*+} D_s^{*-}$ final states. The mass spectra show production of the $J^{PC} = 1^{--}$ states, $\psi(4040)$, $\psi(4160)$ and a weak indication for a smaller enhancement near 4.3 GeV. From fits to the mass spectra for the three different final states we have determined contributions by different $c\bar{c}$ resonances.

Upper limits on $X(4260)$ decays to these final states relative to $J/\psi \pi^+ \pi^-$ are computed. If the $X(4260)$ is a 1^{--} charmonium state, it should decay predominantly to open charm. Within the present limited data sample size, no evidence is found for $X(4260)$ decays to $D_s^+ D_s^-$, $D_s^{*+} D_s^-$, and $D_s^{*+} D_s^{*-}$. If the $X(4260)$ were a tetraquark state, it would decay predominantly to $D_s^+ D_s^-$ [10].

ACKNOWLEDGMENTS

We are grateful for the extraordinary contributions of our PEP-II colleagues in achieving the excellent luminosity and machine conditions that have made this work possible. The success of this project also relies critically on the expertise and dedication of the computing organizations that support BABAR. The collaborating institutions wish to thank SLAC for its support and the kind hospitality extended to them. This work is supported by the U.S. Department of Energy and the National Science Foundation, the Natural Sciences and Engineering Research Council (Canada), the Commissariat à l'Energie Atomique and Institut National de Physique Nucléaire et de Physique des Particules (France), the Bundesministerium für Bildung und Forschung and Deutsche Forschungsgemeinschaft (Germany), the Istituto Nazionale di Fisica Nucleare (Italy), the Foundation for Fundamental Research on Matter (The Netherlands), the Research Council of Norway, the Ministry of Education and Science of the Russian Federation, Ministerio de Ciencia e Innovación (Spain), and the Science and Technology Facilities Council (United Kingdom). Individuals have received support from the Marie-Curie IEF program (European Union), the A. P. Sloan Foundation (USA), and the Binational Science Foundation (USA-Israel).

- [1] S.-K. Choi *et al.* (Belle Collaboration), *Phys. Rev. Lett.* **91**, 262001 (2003).
- [2] B. Aubert *et al.* (BABAR Collaboration), *Phys. Rev. Lett.* **95**, 142001 (2005).
- [3] B. Aubert *et al.* (BABAR Collaboration), *Phys. Rev. Lett.* **98**, 212001 (2007).

- [4] X.L. Wang *et al.* (Belle Collaboration), *Phys. Rev. Lett.* **99**, 142002 (2007).
- [5] T. Barnes, S. Godfrey, and E. S. Swanson, *Phys. Rev. D* **72**, 054026 (2005).
- [6] E.J. Eichten, K. Lane, and C. Quigg, *Phys. Rev. D* **73**, 014014 (2006).

- [7] X. H. Mo *et al.*, *Phys. Lett. B* **640**, 182 (2006).
- [8] S. L. Zhu, *Phys. Lett. B* **625**, 212 (2005); E. Kou and O. Pene, *Phys. Lett. B* **631**, 164 (2005); F. E. Close and P. R. Page, *Phys. Lett. B* **628**, 215 (2005).
- [9] C. F. Qiao, *Phys. Lett. B* **639**, 263 (2006).
- [10] L. Maiani, F. Piccinini, A. D. Polosa, and V. Riquer, *Phys. Rev. D* **72**, 031502 (2005).
- [11] X. Liu, X. Q. Zeng, and X. Q. Li, *Phys. Rev. D* **72**, 054023 (2005).
- [12] E. S. Swanson, *Phys. Rep.* **429**, 243 (2006).
- [13] Charge conjugate states are implied throughout this work.
- [14] B. Aubert *et al.* (BABAR Collaboration), *Phys. Rev. D* **76**, 111105 (2007).
- [15] B. Aubert *et al.* (BABAR Collaboration), *Phys. Rev. D* **79**, 092001 (2009).
- [16] G. Pakhlova *et al.* (Belle Collaboration), *Phys. Rev. D* **77**, 011103 (2008).
- [17] G. Pakhlova *et al.* (Belle Collaboration), *Phys. Rev. Lett.* **98**, 092001 (2007).
- [18] J. Libby *et al.* (CLEO Collaboration), *Nucl. Phys. B, Proc. Suppl.* **181–182**, 127 (2008).
- [19] B. Aubert *et al.* (BABAR Collaboration), *Nucl. Instrum. Methods Phys. Res., Sect. A* **479**, 1 (2002).
- [20] G. Bonneau and F. Martin, *Nucl. Phys.* **B27**, 381 (1971); H. Czyz *et al.*, *Eur. Phys. J. C* **18**, 497 (2001).
- [21] S. Agostinelli *et al.* (GEANT Collaboration), *Nucl. Instrum. Methods Phys. Res., Sect. A* **506**, 250 (2003).
- [22] C. Amsler *et al.*, *Phys. Lett. B* **667**, 1 (2008).
- [23] M. Benayoun *et al.*, *Mod. Phys. Lett. A* **14**, 2605 (1999).
- [24] S. J. Brodsky and C. R. Ji, *Phys. Rev. Lett.* **55**, 2257 (1985).
- [25] J. M. Blatt and V. F. Weisskopf, *Theoretical Nuclear Physics* (Wiley, New York, 1952).